JASMAC
Conference of the Japan Society of Microgravity Appllication

P17

音場浮遊液滴の蒸発および析出プロセス

Evaporation and Precipitation Processes of an Acoustically Levitated Droplet

○丸山 侑太郎 [1]，長谷川 浩司 [2]
○**Yutaro MARUYAMA[1], Koji HASEGAWA[1]**
1 工学院大学大学院工学研究科機械工学専攻，Graduate School of Engineering, Kogakuin University,
2 工学院大学工学部機械工学科，Department of Mechanical Engineering, Kogakuin University

1. Introduction

The acoustic levitation method is one of the contactless manipulation technologies that can suspend a sample in mid-air by forming an acoustic standing wave in the horn and the reflector [1-2]. This levitation method is expected to be applied for a container-less processing in the field of biotechnology, analytical chemistry, material and pharmaceutical sciences. because acoustic levitation method could avoid heterogeneous nucleation and contamination caused by the container wall [2-3]. It is promising to realize the contactless fluid manipulation by acoustic levitation, however, it causes the non-liner behavior. For instance, an evaporation of a levitated droplet is promoted by a non-linear acoustic streaming [4]. Although it is necessary to understand the evaporation and precipitation behavior of multicomponent droplets for perfect sample manipulation with acoustic levitation method, the underlying physics is not sufficiently understood due to complex non-linear behavior.

The purpose of our study is to understand the evaporation and precipitation behaver a levitated multicomponent droplet for contactless sample manipulation via acoustic levitation. In this study, the evaporation and precipitation behaviors of multicomponent droplets via acoustic levitation were experimentally evaluated and compared with the expanded theoretical prediction.

2. Experimental design

Figure 1 shows a schematic of the experimental apparatus. First, a sinusoidal signal is transmitted using the function generator and amplified it with the power amplifier. Then this is inputted to the ultrasonic transducer through the power meter and sound wave is generated from the bottom horn and it reflects on the top reflector. Acoustic standing wave is formed between horn and reflector and the droplet is injected using syringe manually. Droplet can be levitated near a pressure node of the acoustic standing wave. To visualize the behavior of a levitated droplet, we captured levitated droplet by backlight illumination using high-speed camera and the temporal evolution of the surface temperature of a droplet were measured using the radiation thermometer. The obtained images are processed by a computer.

The sine wave generated by the function transmitter had a frequency of approximately 19.3 kHz. The sound pressure of the belly above the suspended droplet, as measured using the probe microphone, was 1.3–1.8 kPa. The test fluids included a salt solution in which edible salt was dissolved in pure water and an NaCl aqueous solution in which NaCl was dissolved. The room temperature was set to 25±2 °C using an air conditioner, and the relative humidity was set to 50±7% using a dehumidifier. The initial droplet diameter was 1.0–2.0 mm. The emissivity for the radiation thermometer was 0.96[5-6].

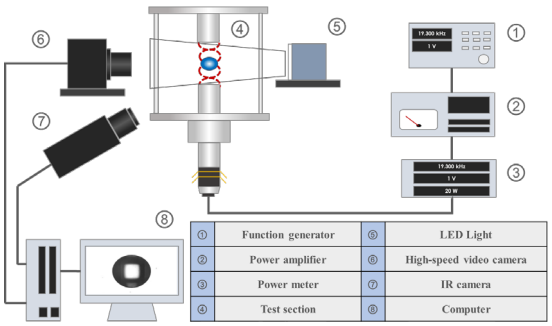

Fig. 1 Schematic of experimental setup.

3. Theory

3.1 Single-component droplets

For non-contact manipulation, it is particularly important to estimate the evaporation of droplets. Therefore, the theoretical and experimental results were compared. The d^2-law,[7] as an equation for the mass transport of single-component droplets, is widely used in the estimation of the evaporation of single-component droplets, and it can be expressed as follows.

$$\left(\frac{d}{d_0}\right)^2 = 1 - \frac{8DM}{\rho_l R}\left(\frac{P_s}{T_s} - \frac{P_\infty}{T_\infty} \times \frac{RH}{100}\right)\frac{t}{{d_0}^2} \tag{1}$$

where D is the diffusion coefficient, M is the molecular weight, ρ_l is the density, R is the gas constant, P is the vapor pressure, T is the temperature, RH is the relative humidity, t is the time, and d_0 is the initial equivalent diameter of the droplet. The subscript *sur* represents the droplet surface and ∞ represents the ambient gas.

3.2 Multi-component droplet with vapor pressure depression

Based on Eq. (1), Combe and Donaldson applied the d^2-law in a form corresponding to the evaporation process of the acoustic levitated droplets involving precipitation.[8] In the solutions containing non-volatile solutes, the vapor pressure depends on the molar fraction of the solute. Therefore, the d^2-law considering the molar fraction of the solute can be presented as in Eq. (2).

$$\left(\frac{d}{d_0}\right)^2 = 1 - \frac{8DM}{\rho_l R}\left(\frac{P_{sur}(1 - i \cdot Z_s)}{T_{sur}} - \frac{P_\infty}{T_\infty} \times \frac{RH}{100}\right)\frac{t}{{d_0}^2} \tag{2}$$

where Zs is the solute molar fraction, and i is the van't Hoff factor.

4. Results and discussion

4.1 General observation

The evaporation process and surface temperature were observed using a solution involving salt mixed with pure water. **Figure 2(a)** shows the evaporation process of the salt solution and water with the visualization images at each time by using the salt solution (20 wt%). The horizonal axis represents the time, and the vertical axis represents the squared droplet diameter normalized by the squared initial droplet diameter. The initial droplet diameters d_0 of the salt solution and water were 1.5 mm and 1.7 mm, respectively. In stage I, the evaporation process of the water droplets was linear, in which the dimensionless surface area decreased by approximately 50% in 900 s. The evaporation process of the salt solution involved vaporization up to approximately 1500 s, and the dimensionless surface area decreased by approximately 60% at 1500 s. Subsequently, in stage II, the reduction in the dimensionless surface area was nearly eliminated, and the area became constant. This phenomenon occurred because the water component of the salt solution evaporated over time, and it was completely evaporated at approximately 1500 s. Such a two-stage evaporation process was likely occurred because the precipitation salt remained in the solution.

Figure 2(b) shows the measurement results of the interface temperature of a salt solution droplet. At the time of droplet injection, the temperature was approximately 24 °C, which is 1 °C lower than the outside temperature. Subsequently, although the surface temperature of the salt solution did not exhibit a significant change until approximately 1500 s, it increased to approximately 27 °C from 1500 s to 1605 s and then became constant. The reasons for the increase in temperature between 1500 s and 1605 s and subsequent constancy are believed to be the evaporation of the water component and complete precipitation of the salt. The reason for the surface temperature becoming constant at a temperature 2 °C higher than the room temperature is thought to be due to a deviation from the initial emissivity of 0.96 (calibrated for initial multicomponent droplets), owing to the complete precipitation of the salt. These results indicate that the salt was completely deposited in 1500 s, and the salt could be precipitated in a levitated state.

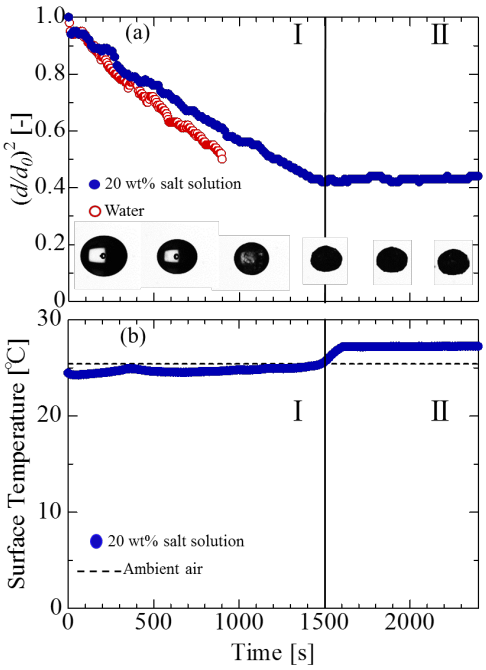

Fig. 2 Evaporation and precipitation process of the levitated droiplet:
(a) Water and salt solution droplet with snapshots (b) Surface temperature of the salt solution droplet.

4.2 Effect of initial concentration

Figure 3(a) shows the evaporation process at each initial concentration of 10 wt%, 15 wt%, 20 wt%, and 25 wt% for an initial droplet diameter d_0 of 1.7 mm, 1.7 mm, 1.8 mm, and 1.8 mm, respectively. As the initial concentration increased, the evaporation of the droplet reduced, likely because the evaporation was suppressed by the vapor pressure depression that increased the initial concentration. **Figure 3(b)** shows the time taken for the complete salt precipitation at each initial concentration. The horizontal axis in the figure represents the initial salt concentration, and the vertical axis represents the time at which the salt was completely precipitated. The images in the figure are examples of the visualized image at each density. Although the precipitation time was considered to be reduced owing to the decrease in the volume of the water concentration with an increase in the salt concentration (the precipitation time was approximately 1860 s, 1800 s, 1710 s, and 1710 s at 10 wt%, 15 wt%, 20 wt%, and 25 wt%, respectively), no significant change in the precipitation time was observed with a change in the salt concentration. The precipitation time was not reduced likely because the evaporation rate was retarded due to the vapor pressure depression when the salt concentration increased. The visualization images at the time of precipitation indicate that for the salt concentrations of 10 wt% and 15 wt%, the precipitation occurred in a nearly spherical shape, whereas for 20 wt% and 25 wt%, the precipitation shape was closer to an ellipsoid. The shapes are considered to be attributed to the influence of the internal circulation driven by nonlinear sound waves.[9-10)]

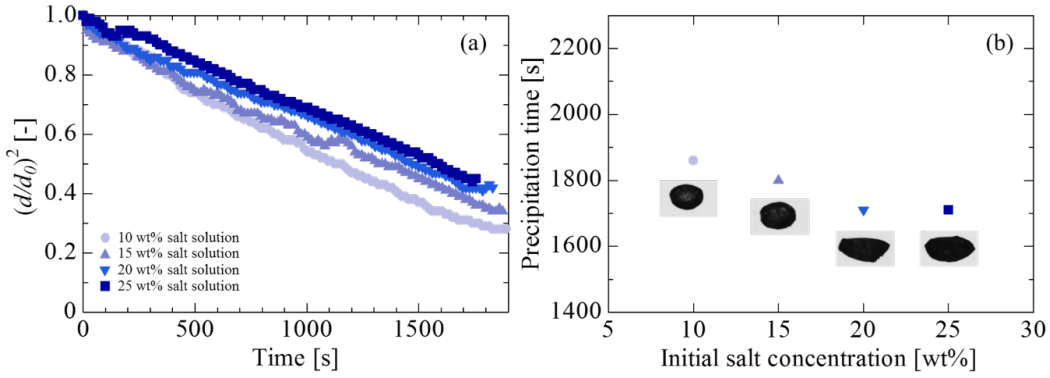

Fig. 3 Effect of initial concentration on the droplet evaporation and precipitation: (a) Evaporation process of the salt solution. (b) Precipitation time and final shape of salt.

4.3 **Comparison with theory**

The evaporation process of the salt solution was compared with the theory represented by Eq. (1). For the surface temperature of the droplet, the experimental data in **Fig. 2(b)** were substituted, and the physical properties of water were used to determine the diffusion coefficient and density of the levitated samples. **Figure 4** presents the comparison between the experimental results and the theoretical prediction. The solid line in the figure indicates the theoretical values obtained using Eq. (1). The experimental data were considerably different from the theoretical values, likely because of the effect of the vapor pressure depression due to the dissolution of the non-volatile substances. It is considered that the salt solution was separated because the evaporation rate was lower than that of pure water, owing to the vapor pressure depression. Therefore, it is necessary to expand Eq. (1) to take into account the vapor pressure depression.

Consequently, we compared the extended theory represented by Eq. (2) with the experimental results, considering the vapor pressure depression. The green dashed line in **Figure 4** shows a comparison between the theoretical and experimental values, considering the vapor pressure drop of the initial concentration. *Zs* was calculated using the initial solute concentration of 20 wt% in the salt solution, and the concentration change with time was not considered. In the calculation, it was assumed that the salt was NaCl, and i was 2[8]. The experimental data and theoretical prediction agreed up to approximately 345 s; however, these values exhibited a discrepancy thereafter. This phenomenon is considered to be because the vapor pressure further decreased due to the increase in the concentration accompanying the evaporation of the salt solution, and the experimentally obtained evaporation rate reduced. For a better prediction of the evaporation kinetics, the concentration change with time was estimated. First, the mass of the water component and salt contained in the saline droplet were calculated using Eqs. (3) and (4), respectively.

$$m_s = \rho_s \frac{4}{3}\pi\left(\frac{d_0}{2}\right)^3 \times \frac{x_s}{100} \tag{3}$$

$$m_w = \rho_w \frac{4}{3}\pi\left(\frac{d_0}{2}\right)^3 \times \frac{(1-x_s)}{100} \tag{4}$$

where ρ is the density of the NaCl aqueous solution, d_0 is the initial droplet diameter, and x is the initial concentration of the solute. The subscripts s and w represent the salt and water components, respectively. The experimental results indicated that the salt solution was completely precipitated in 1500 s; consequently, the mass of each component at each time was calculated such that the mass of the water component evaporated in 1500 s. Eq. (5) shows the formula to calculate the mass fraction used.

$$Y_s = \frac{m_s}{m_s + m_w} \tag{5}$$

Figure 5 shows the estimation of the salinity at each time. Because the solubility of sodium chloride in water was approximately 26.4 wt%, it was estimated that the water was saturated at approximately 450 s, and the water was completely evaporated by 1500 s. Based on this experimental data, the time evolution of the mass fractions up to 450 s (saturation of sodium chloride in water) was estimated in the present study. To obtain a clear insight into the evaporation kinetics of the levitated droplet, we calculated the evaporation process considering the vapor pressure depression by using Eq. (2). The red dashed line in **Fig. 4** shows the theoretical value calculated using Eq. (2). Although the theoretical was in partial agreement with the experimental value up to approximately 510 s, the two values exhibited considerable differences thereafter. A probable reason could be the presence of the precipitated salt on the droplet surface after the supersaturation of the salt solution.

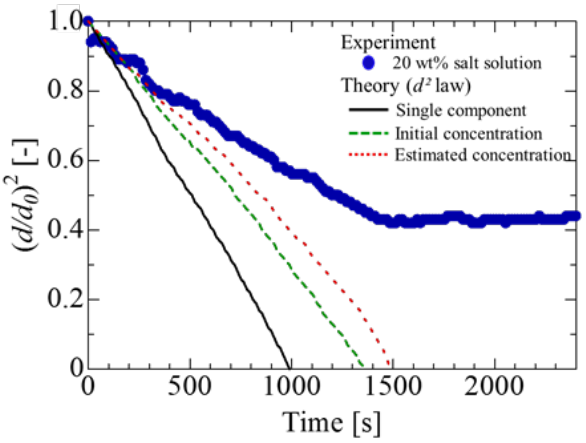

Fig. 4 Comparison of experimental data and theoretical prediction.

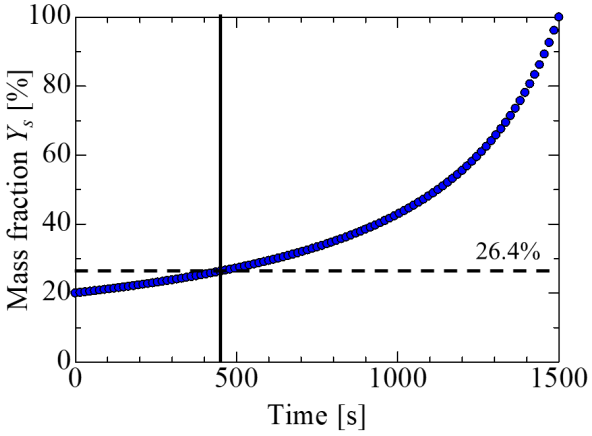

Fig. 5 Estimation of mass concentration in the levitated salt solution droplet.

4.4 Time estimation for complete salt precipitation

The prediction of the evaporation and precipitation time of the levitated sample is of considerable importance for the application of the ALM in the field of chemical engineering. Thus, the precipitation time was estimated using the d^2-law, considering the solute mole fraction. In Eq. (2), when the droplet diameter is $d = 0$ mm, the water component of the droplet completely evaporates. Therefore, the precipitation time (complete evaporation of water) t can be estimated using $d = 0$ mm. Eq. (6) is used to determine the theoretical evaporation constant β, obtained by Eq. (2).

$$\beta = \frac{8DM}{\rho_l R}\left(\frac{P_{sur}(1 - i \cdot Z_s)}{T_{sur}} - \frac{P_\infty}{T_\infty} \times \frac{RH}{100}\right)\frac{t}{{d_0}^2} \tag{6}$$

Substituting Eq. (7) and $d = 0$ mm into Eq. (2) and solving for t leads to the precipitation time t_p, as shown in Eq. (7).

$$t_p = \frac{{d_0}^2}{\beta} \tag{7}$$

Figure 6 shows a comparison of the precipitation time estimated using the theory of droplets with precipitation and the experimentally obtained precipitation time. The horizontal axis represents the experimental values, and the vertical axis represents the theoretically estimated precipitation time. The experimental value was calculated considered the instant at which the salt was completely precipitated and the volume equivalent diameter did not decrease during the evaporation process. The theoretical predictions were in good agreement with the experimental results. It could be concluded that the precipitation time, when the water component completely evaporates, can be predicted using Eqs. (6) and (7).

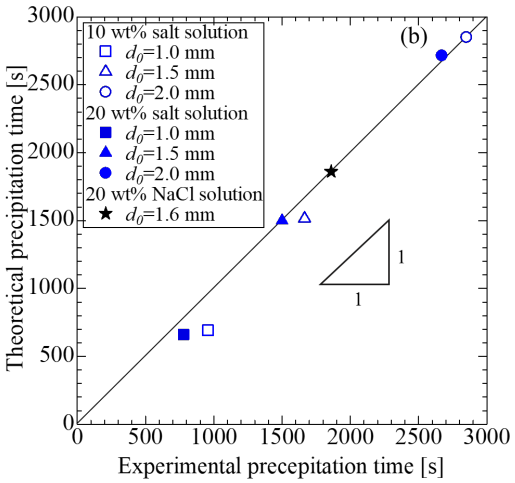

Fig. 6 Comparison of experimental data and theoretical precipitation time of salt solution and NaCl solution.

5. Conclusions

In this study, the evaporation and precipitation behaviors of multicomponent droplets via acoustic levitation were experimentally evaluated and compared with the expanded theoretical prediction. The salt solution droplets exhibit a two-stage evaporation process, involving water evaporation and salt precipitation. A higher concentration led to a lower droplet evaporation rate. Because of the vapor pressure depression, the experimental data disagreed with the classical theoretical prediction obtained using the d^2-law. The experimental results and those obtained using the d^2-law exhibited partial agreement when the vapor pressure depression with the concentration estimation at each time was considered using the experimental data. In addition, the precipitation time, when the water was completely evaporated, was well-predicted using the extended theory.

References

1) V. Vandaele and P. Lambert: Precis. Eng., **29** (2005) 491.
2) D. Foresti, M. Nabavi, M. Klingauf, A Ferrari and D. Poulikakos: PNAS, **110** (2013) 12549.
3) W. J. Xie, C. D. Cao, Y. J. Lu and B. Wei: Phys. Rev. E, **66** (2002) 61601.
4) A. L. Yarin, G. Brenn, O. Castner, D. Rensink and C. Tropea: Journal of Fluid Mechanics, **399** (1999) 151.
5) P. Vázquez, C. T. Schneider, K. Mouhoubi, G. Fronteau, M. Gommeaux, D. Benavente, V. Barbin and J. L. Bodnar: Infrared Phys. Technol., **71** (2015) 198.
6) R. Tuckermann, S. Bauerecker and H. K. Cammenga: Int. J. Thermophys.,**25** (2005) 1583.
7) A. Frohn and N. Roth: Dynamics of droplets: Springer Science and Business Media, (2000).
8) N. A. Combe and D. J. Donaldson: J. Phys. Chem. A , **7** (2017) 7204.
9) Y. Yamamoto, Y. Abe, A. Fujiwara, K. Hasegawa and K. Aoki: *Microgravity. Sci. Technol.*, **20** (2008) 277.
10) Y. Sasaki, K. Kobayashi, K. Hasegawa, A. Kaneko and Y. Abe: *Phys. Fluids*, **31** (2019) 102109.